Letter

Neutron magicity in the proton drip-line nucleus ^{20}Mg: First invariant-mass reconstruction of ^{19,20}Mg

L. Ni,[1,*] Y. Jin,[1,*] Z. H. Li,[1,†] K. W. Brown,[2,3,‡] C. X. Yuan,[4] H. Hua,[1,§] C. Y. Niu,[2] A. K. Anthony,[2,5,‖] J. Barney,[2,5] R. J. Charity,[6] D. Dell'Aquila,[2,¶] J. M. Elson,[6] J. Estee,[2,5] G. Jhang,[2] J. G. Li,[7,8] W. G. Lynch,[2,5] N. Michel,[7,8] L. G. Sobotka,[6,9] S. Sweany,[2,5] F. C. E. Teh,[2,5] A. Thomas,[6] C. Y. Tsang,[2,5] M. B. Tsang,[2,5] S. M. Wang,[10,11] H. Y. Wu,[1] and K. Zhu[2,5]

[1]*School of Physics and State Key Laboratory of Nuclear Physics and Technology, Peking University, Beijing 100871, China*

[2]*Facility of Rare Isotope Beams, Michigan State University, East Lansing, Michigan 48824, USA*

[3]*Department of Chemistry, Michigan State University, East Lansing, Michigan 48824, USA*

[4]*Sino-French Institute of Nuclear Engineering and Technology, Sun Yat-Sen University, Zhuhai 519082, China*

[5]*Department of Physics and Astronomy, Michigan State University, East Lansing, Michigan 48824, USA*

[6]*Department of Chemistry, Washington University, Saint Louis, Missouri 63130, USA*

[7]*Institute of Modern Physics, Chinese Academy of Sciences, Lanzhou 730000, China*

[8]*School of Nuclear Science and Technology, University of Chinese Academy of Sciences, Beijing 100049, China*

[9]*Department of Physics, Washington University, Saint Louis, Missouri 63130, USA*

[10]*Key Laboratory of Nuclear Physics and Ion-beam Application (MOE), Institute of Modern Physics, Fudan University, Shanghai 200433, China*

[11]*Shanghai Research Center for Theoretical Nuclear Physics, NSFC and Fudan University, Shanghai 200438, China*

(Received 12 August 2024; accepted 7 November 2024; published 5 December 2024)

The resonant states in ^{20}Mg and ^{19}Mg have been studied by the invariant-mass reconstruction of ^{18}Ne $+2p$ and ^{17}Ne $+2p$ events, respectively. Two new resolved states (4_1^+ and 2_2^+) in ^{20}Mg are found to decay through ^{19}Na intermediate states to the ground state of ^{18}Ne from the examination of the decay-energy spectra for ^{18}Ne $+1p$ subsystems. The deduced $R_{42} = E^*(4_1^+)/E^*(2_1^+)$ ratio of 2.10(1) is close to the expected harmonic-vibrator value and reveals a spherical or weakly deformed shape for ^{20}Mg. Systematic comparison of $E^*(2_1^+)$ and R_{42} along isotopic and isotonic chains with shell model calculations, using the YSOX interaction, suggest the persistence of $N = 8$ shell around the proton drip-line. The relatively higher 2_1^+ excitation energy in ^{18}Mg relative to ^{20}Mg can be ascribed to different excitation characters of the valence protons. The $1/2_1^+$ state in ^{19}Mg has been observed for the first time. The energy differences between the $1/2_1^-$ and $1/2_1^+$ states in ^{19}Mg and its isotones manifest the magnitude of the $N = 8$ shell gap on the proton-rich side.

DOI: 10.1103/PhysRevC.110.L061301

Since the shell model (SM) was proposed by Mayer [1] and Haxel, Jensen, and Suess [2], there has been an intense effort to study the evolution of nuclear shell structure across the nuclear chart. With the recently acquired capability to study nuclei far from the line of β stability, some traditional magic numbers [3–10], $N = 8$, 20, and 28, have been found to disappear in neutron-rich regions, with the emergence of new ones [11–24] at $N = 14$, 16, 32, and 34. Detailed descriptions of these findings can be found in the reviews of Refs. [25–27].

Long isotopic chains extending into the neutron-rich region have enabled extensive study of the shell evolution of this side of stability. Far less is known on the proton-rich side. One intriguing result on the proton-rich side is the breakdown of the $Z = 8$ shell closure, which is indicated by the lowered location of the 2_1^+ or 0_2^+ state in the proton-unbound nucleus ^{12}O [28], an effect ascribed to the proton-neutron monopole interaction [28,29]. Two recent experimental studies have suggested a possible weakening of the $N = 8$ shell closure near the proton drip-line. In one study, a considerable quadrupole deformation in ^{20}Mg was extracted from an inelastic deuteron scattering experiment [30]. In another study, using the invariant-mass method, a higher excitation energy of the 2_1^+ state is found in ^{18}Mg ($N = 6$) than in ^{20}Mg ($N = 8$) [31]. Mean-field [32–42] and beyond-mean-field [43] calculations predict neither that ^{20}Mg is significantly deformed nor a weakening of the $N = 8$ shell, while the macroscopic-microscopic model [44] and a Hartree-Fock calculation, neglecting the pairing correlation [45], do suggest that ^{20}Mg is deformed.

So far, the spectroscopic information for the Mg isotopes around $N = 8$ is scarce. For ^{20}Mg only two resonant structures, including a relatively wide peak at $E^* = 3.70$ MeV,

*These authors contributed equally to this work.
†Contact author: zhli@pku.edu.cn
‡Contact author: brownk@frib.msu.edu
§Contact author: hhua@pku.edu.cn
‖Present address: Department of Physics and Astronomy, High Point University, High Point, NC 27268, USA.
¶Present address: Department of Physics "Ettore Pancini", University of Naples "Federico II" & INFN-Naples, Naples 80138, Italy.

have been reported [30]. It is interesting to note that the resonant structures of ^{20}Mg play a pivotal role not only in determining the fate of $N = 8$ shell but also in estimating the reaction rate of ^{18}Ne$(2p, \gamma)^{20}$Mg, which is a potential breakout reaction from the hot CNO cycle in type-I x-ray bursts [46,47]. In this Letter, we report on spectroscopic studies of ^{20}Mg and ^{19}Mg using the invariant-mass method. The deduced $R_{42} = E^*(4_1^+)/E^*(2_1^+)$ ratio for ^{20}Mg and the energy difference between the $1/2_1^-$ and $1/2_1^+$ states in ^{19}Mg suggest the persistence of the $N = 8$ shell around the proton drip-line.

The experiment was performed at the National Superconducting Cyclotron Laboratory at Michigan State University. A primary beam of ^{24}Mg was accelerated through the Coupled Cyclotron Facility to $E/A = 170$ MeV and fragmented on a ^{9}Be primary target. A secondary beam of ^{20}Mg at $E/A = 103$ MeV was then selected with the A1900 fragment separator [48,49]. This secondary beam had an intensity of 5600 pps and a purity of 31%. Particle identification of these secondary beam particles was achieved on an event-by-event basis via their time of flight between two plastic scintillators. The ^{20}Mg beam impinged on a 1-mm-thick secondary ^{9}Be target, producing ^{20}Mg and ^{19}Mg resonant states via projectile inelastic-excitation reactions and one-neutron knockout reactions, respectively. These unstable states promptly decayed, and the ^{18}Ne $+2p$ and ^{17}Ne $+2p$ decay channels were investigated. After passing through a 6-mm-thick aluminum absorber, the protons were detected by an array of ΔE-E telescopes subtending 1.2° to 10.1° in the laboratory and consisting of an annular 1-mm-thick double-sided silicon-strip detector [50] followed by an annular array of CsI(Tl) crystals. The CsI(Tl) array was composed of 20 50-mm-thick crystals, arranged in two concentric rings with 4 and 16 detectors in the inner and outer rings, respectively.

Most of the ^{18}Ne and ^{17}Ne residues passed through a 10-mm-diameter hole in the center of the ΔE-E telescope and then through two orthogonal ribbons of scintillating fiber. Each ribbon was comprised of 64 fibers each with square (0.25×0.25 mm^2) cross sections. One end of each fiber was coupled to an element of an 8×8 multianode photomultiplier that was read out from its four edges with a resistor network. This scintillating-fiber array (SFA) provides the hit position of the residue close to the location of proton detection, which improves the invariant-mass resolution by accurately measuring the relative angles between the exit-channel fragments. After traversing the SFA, the residues entered the S800 spectrograph [51,52] where the particles were identified with their energies being determined. Previous results from this experiment pertaining to the structure of ^{18}Mg have been published [31].

The decay-energy E_T spectra of ^{20}Mg and ^{19}Mg resonances from the invariant mass of all detected ^{18}Ne $+2p$ and ^{17}Ne $+2p$ events, respectively, are shown in Fig. 1. Four and five peaks can be resolved above a smooth background for ^{20}Mg and ^{19}Mg, respectively. Red curves show fits to these spectra with Breit-Wigner intrinsic line shapes modified by the simulated experimental resolution as in Ref. [31]. The fitted decay energies, excitation energies, and intrinsic decay widths of these states are listed in Table I.

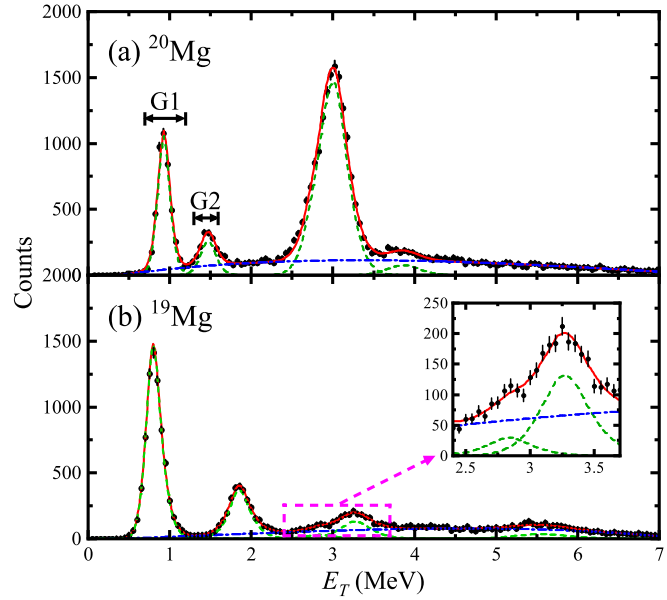

FIG. 1. Decay energy E_T spectra for all detected (a) ^{18}Ne $+2p$ and (b) ^{17}Ne $+2p$ events. The solid-red curves show the fitted spectra along with the contributions of each state (dashed-green curves) and the smooth background (dashed-dotted-blue curves). The inset in panel (b) highlights the region around $E_T = 3$ MeV of panel (b).

For ^{20}Mg, the decay paths of the prominent ^{20}Mg $\rightarrow$ ^{18}Ne $+2p$ resonances observed in Fig. 1(a) were studied by examination of the decay-energy spectra of the ^{18}Ne $+1p$ subsystem. As examples, the spectra of the first two resonant states, which are selected using the gates G1 and G2 in Fig. 1(a), are shown in Figs. 2(a) and 2(b), respectively.

For the first resonant state at $E_T = 0.930$ MeV, the ^{18}Ne $+1p$ subsystem displays two peaks at 0.315 and 0.615 MeV. The lower energy of these corresponds to the decay energy of the ground state of ^{19}Na [see the inset in Fig. 2(a)]. This ^{20}Mg state can thus be understood to undergo a sequential two-proton decay. The first proton decay leads to this ^{19}Na intermediate state which then proton decays to the ground state of ^{18}Ne. This scenario is also confirmed by a simulation of this decay, as shown by the solid red curve in Fig. 2(a). The second ^{20}Mg resonant state, at $E_T = 1.468$ MeV, decays differently. Two peaks at 0.467 and 1.001 MeV

TABLE I. Decay energies E_T, excitation energies E^*, and intrinsic widths Γ of the resonant states in ^{20}Mg and ^{19}Mg. All the values are expressed in MeV. Excitation energies of ^{20}Mg are based on experimental ground-state energy [53].

^{20}Mg			^{19}Mg		
E_T	E^*	Γ	E_T	E^*	Γ
0.930(2)	3.348(3)	0.019(30)	0.794(1)	0	0.000(70)
1.468(5)	3.886(5)	0.045(60)	1.844(3)	1.050(3)	0.015(50)
3.008(2)	5.426(3)	0.209(90)	2.82(1)	2.03(1)	0.00(7)
3.91(2)	6.33(2)	0.07(17)	3.26(1)	2.47(1)	0.04(15)
			5.54(3)	4.75(3)	0.00(4)

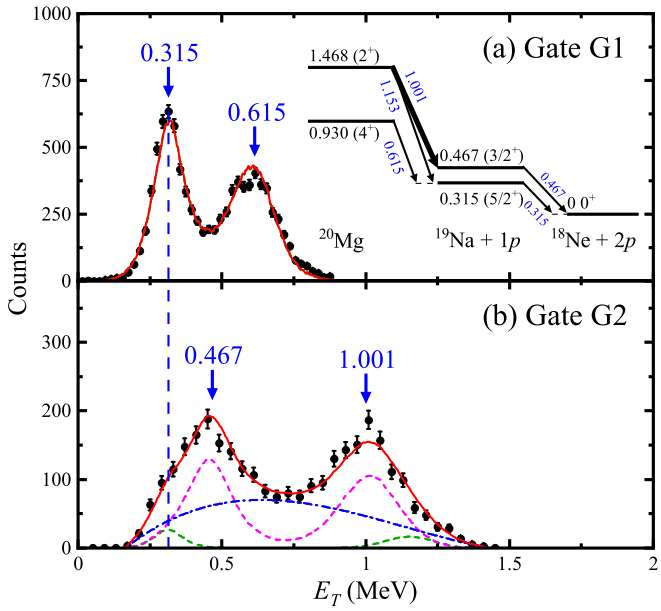

FIG. 2. Decay energy E_T spectra for the ^{18}Ne $+1p$ subsystem with the gates on (a) $E_T = 0.930$ MeV (G1) and (b) 1.468 MeV (G2) resonant states in ^{20}Mg. Red lines are the results of simulations, assuming sequential decay for the resonant states in ^{20}Mg resulting from decay paths through the state at $E_T = 0.315$ MeV in ^{19}Na (dashed-green curve) and the state at $E_T = 0.467$ MeV in ^{19}Na (dashed-magenta curve). A smooth background (dashed-dotted-blue curve) is added in panel (b) because of the relatively high background contribution under the $E_T = 1.468$ MeV state as shown in Fig. 1(a). The shape of the background reflects the distribution when gating outside of the location of the resonances. The blue arrows with numbers and the dashed-blue vertical line show the positions of decay energies in MeV. The inset in panel (a) shows the main decay paths of the first two resonant states in ^{20}Mg. The energies of the states in ^{20}Mg and ^{19}Na relative to the $2p$ and $1p$ thresholds, respectively, are listed on the levels in MeV. The energies of the intermediate states in ^{19}Na are consistent with the available experimental results [54–56]. The blue numbers in the inset are the $1p$ decay energies in MeV between the corresponding states. The bold arrow is the main decay branch of the 1.468-MeV state in ^{20}Mg.

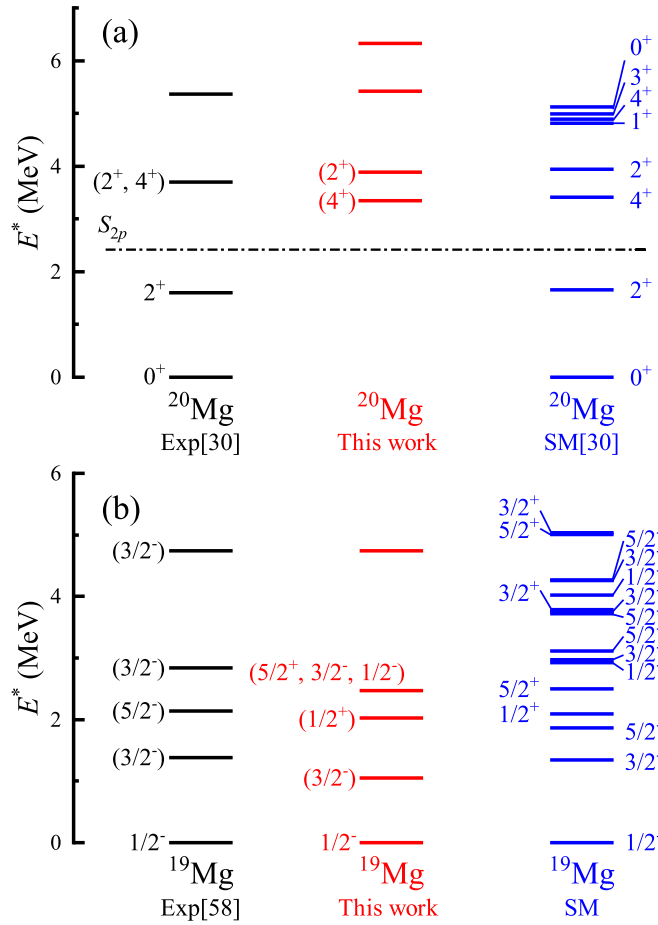

FIG. 3. The excitation energies E^* of (a) the four resonant states in ^{20}Mg and (b) the five resonant states in ^{19}Mg identified in this work (in red). The previous experimental results of ^{20}Mg [30] and ^{19}Mg [58] (in black) and shell model calculations (in blue) for ^{20}Mg from Ref. [30] and for ^{19}Mg are given for comparison. The dashed-dotted line in panel (a) indicates the two-proton separation energy S_{2p} of ^{20}Mg.

are observed in the ^{18}Ne $+1p$ subsystem in Fig. 2(b). These peaks indicate a sequential $2p$ decay process where the ^{19}Na intermediate state is now the first excited state at $E_T = 0.467$ MeV [see the inset in Fig. 2(a)]. This ^{19}Na excited state also proton decays to the ground state of ^{18}Ne. The fit to this spectrum is improved if a minor sequential $2p$ decay branch through the intermediate state at $E_T = 0.315$ MeV in ^{19}Na is included. The third resonant state at $E_T = 3.008$ MeV in ^{20}Mg is found to overwhelmingly decay through the ^{19}Na ground state at $E_T = 0.315$ MeV, which is similar to the first resonant state and is not shown here.

In Fig. 3(a), the excitation energies of the four resonant states in ^{20}Mg observed in this work are compared with the experimental results of Ref. [30] and with the SM calculations therein. The previous experiment observed two resonant structures in ^{20}Mg and the relative wide resonant peak at $E^* = 3.70$ MeV was suggested to be composed of an overlap of the 4^+_1 and 2^+_2 states [30]. As shown in Fig. 1(a), the higher resolution of the present work allows these two states to be fully resolved. Their energies are in good agreement with both the SM predictions from Ref. [30] [see Fig. 3(a)] and the mirror systematics ($E^*(4^+_1) = 3.570$ MeV and $E^*(2^+_2) = 4.072$ MeV in the mirror nucleus ^{20}O [57]). The present spin-parity (4^+ and 2^+) assignments for these two resonant states in ^{20}Mg are consistent with their decay paths [see the inset in Fig. 2(a)]: the higher-spin state 4^+ is likely to preferentially decay to the $(5/2^+)$ ground state of ^{19}Na, while the lower-spin state 2^+ tends to rather decay to the $(3/2^+)$ state in ^{19}Na. The third resonant state observed here is also in fair agreement with the higher-lying state observed in Ref. [30].

For ^{19}Mg, five resonant states were observed in the previous experimental works utilizing the in-flight decay method, all of which were assumed to decay to the ground state in ^{17}Ne [58–62]. Here, the decay paths of the first two resonances of ^{19}Mg, which have high statistics, are investigated by examination of the decay-energy spectra of the ^{17}Ne $+1p$

TABLE II. The theoretical and experimental excitation energies and yields relative to the ground state for low-lying resonant states ($E^* < 3.0$ MeV) in ^{19}Mg. The excitation energies are in MeV.

Experimental		Theoretical			
E^*	σ_{exp}	E^*	σ_{th}	Configuration	J^π
0	1	0	1	$1p_{1/2}$	$1/2^-$
1.050	0.320(8)	1.341	0.156	$1p_{3/2}$	$3/2^-$
2.03	0.032(6)	2.085	0.016	$2s_{1/2}$	$1/2^+$
2.47	0.214(9)	2.498	0.042	$1d_{5/2}$	$5/2^+$
		2.922	0.029	$1p_{1/2}$	$1/2^-$
		2.971	0.086	$1p_{3/2}$	$3/2^-$

subsystem [63] and found to be consistent with the conclusions in Refs. [58–62].

The comparison between the experimental states of ^{19}Mg observed in this work and previous experiments [58–62], as well as with our SM calculations, is shown in Fig. 3(b). The SM calculations are performed in the *psd* model space with the YSOX interaction [64], which have been successfully applied to describe properties of loosely bound proton-rich nuclei around $A = 20$ [65]. In Fig. 3(b) it can be seen that the resonant structures observed in the present work well agree with the SM calculations and are consistent with those reported in previous experimental studies except for the spin-parity assignment for the second excited state at $E^* = 2.03$ MeV.

The second excited state at $E^* = 2.03$ MeV of ^{19}Mg was tentatively assigned as $5/2^-$ in Ref. [58]. In both that and the present work, ^{19}Mg was produced by one-neutron knockout from ^{20}Mg. As the neutron population of the $f_{5/2}$ orbit in ^{20}Mg$_{g.s.}$ is marginal, the population of a low-lying $5/2^-$ state in ^{19}Mg should be very weak in both this work and that of Ref. [58].

The relative reaction cross sections for populating resonant states in ^{19}Mg were calculated from a Glauber model of nucleon knockout (MOMDIS code) [66] with the SM spectroscopic factors. The theoretical and experimental yields for low-lying resonant states relative to the ground state in ^{19}Mg are listed in Table II. This comparison indicates that a spin-parity of $1/2^+$, corresponding to the knockout of an $s_{1/2}$ neutron, is a reasonable assignment for the second excited state ($E^* = 2.03$ MeV) of ^{19}Mg. As for the third excited state at $E^* = 2.47$ MeV, the SM plus MOMDIS calculations indicate that $5/2^+$, $3/2^-$, and $1/2^-$ are all possible.

Figures 4(a) and 4(b) display the excitation energies for the 2_1^+ states in even-even $Z = 10$ and 12 isotopes and $N = 10$ and 12 isotones, respectively. For the $N = 10$ and 12 isotones [Fig. 4(b)], the 2_1^+ energies peak at $Z = 8$. Mirror symmetry is seen in the $Z = 10$ isotopic chain [Fig. 4(a)], which also has a maximum at $N = 8$. Deviating from this systematics is ^{20}Mg ($N = 8$), where its 2_1^+ energy is lower than that of ^{18}Mg ($N = 6$) [31].

As previously mentioned, considerable deformation in ^{20}Mg, and consequently a deformation-driven weakening of the $N = 8$ shell closure at the proton drip-line, was suggested in Ref. [30]. Fixing the excitation energy of the 4_1^+ state

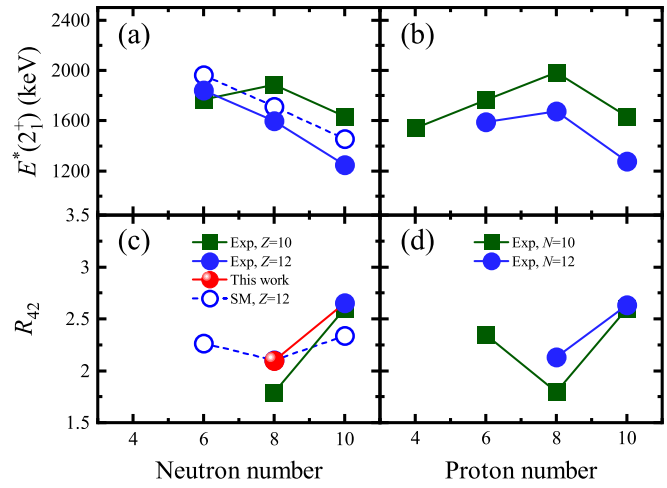

FIG. 4. (a) $E^*(2_1^+)$ and (c) R_{42} ratios for $Z = 10$ and 12 isotopes. (b) $E^*(2_1^+)$ and (d) R_{42} ratios for $N = 10$ and 12 isotones. Experimental data are taken from Ref. [67] and this work. The SM calculations for (a) $E^*(2_1^+)$ and (c) R_{42} in Mg isotopes are given for comparison.

in ^{20}Mg offers a straightforward method for investigating whether ^{20}Mg is deformed. Systematics for the ratio of the excitation energies of the 4_1^+ and 2_1^+ states, R_{42}, are shown in Fig. 4(c) for $Z = 10$ and 12 isotopes and Fig. 4(d) for $N = 10$ and 12 isotones. Lower R_{42} ratios at $Z(N) = 8$ are observed for all four chains [67,68]. For a deformed rigid rotor, $R_{42} \approx 3.3$, while for purely spherical vibrational nuclei this ratio should be equal to 2. The relatively low R_{42} ratio of 2.10(1) suggests a near spherical shape for ^{20}Mg at $N = 8$ and argues against a deformation-driven weakening of the $N = 8$ shell closure at the proton drip-line. This experimental result is consistent with both mean-field [32–42] and beyond-mean-field [43] calculations. SM calculations are compared to the experimental results in Fig. 4, where it can be seen that the calculations reproduce the experimental trends. Specifically, a minimum in R_{42} is predicted at ^{20}Mg, indicating a shell closure at $N = 8$.

The new spectroscopy of ^{19}Mg provides more insight into the evolution of the $N = 8$ shell at the proton drip-line. The YSOX SM calculations suggest an inversion of the $1/2^+$ and $5/2^+$ states occurs in ^{19}Mg [Fig. 3(b)] compared with ^{21}Mg, which indicates the crossing of the $\nu 2s_{1/2}$ and $\nu 1d_{5/2}$ neutron orbitals.

The lowering in energy of the $1/2^+$ state (compared to the $5/2^+$ state) has also been found in all $N = 7$ isotones from $Z = 2$ to $Z = 10$ [5,69–72]. Consequently, the energy differences $\Delta E_{1/2}$ between the lowest-lying $1/2^+$ and $1/2^-$ states (originating from $\nu 2s_{1/2}$ and $\nu 1p_{1/2}$ orbitals, respectively) in $N = 7$ isotones can provide valuable information on the magnitude of the $N = 8$ shell gap. In Fig. 5, $\Delta E_{1/2}$ values are negative at the neutron drip-line ($Z \leqslant 4$), indicating the $\nu 2s_{1/2}$ level is intruding into the p shell. This causes a breakdown of the normal shell ordering and has been confirmed for He [73], Li [74,75], Be [5,7,76–79], and B [80]. The maximum of $\Delta E_{1/2}$ at $Z = 8$ reflects the proton magicity [25]. The robustness of the $N = 8$ shell closure in neon isotopes has been verified [68] [also seen here in Fig. 4(a)]. The same

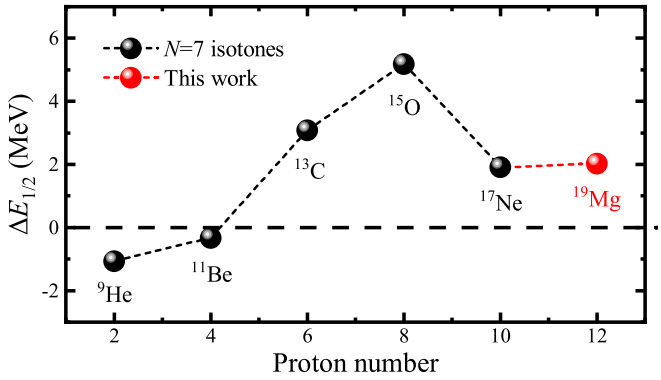

FIG. 5. Systematics of experimental energy differences $\Delta E_{1/2}$ between the lowest-lying $1/2^+$ and $1/2^-$ states in $N = 7$ isotones. Data are taken from Refs. [67,69,72] and this work.

is true for carbon isotopes [25]. The similar $\Delta E_{1/2}$ values for ^{17}Ne and ^{19}Mg in Fig. 5, the magnitudes of which are only a little smaller than the value for ^{13}C (which has the $Z = 6$ subshell closure), further support the persistence of the $N = 8$ shell near the proton drip-line and the magicity of ^{20}Mg.

The persistence of the $N = 8$ shell in Mg isotopes suggests that the 2_1^+ states in even-even ^{20}Mg and ^{18}Mg mainly arise from the excitation of valence protons. The proton effective single-particle energies of Mg isotopes are calculated by the SM and an inversion of $\pi 2s_{1/2}$ and $\pi 1d_{5/2}$ orbitals is predicted to occur between ^{20}Mg and ^{18}Mg. This inversion can be attributed to the nucleon-nucleon monopole interactions [26] with the decreased occupancy of two $1p_{1/2}$ neutrons in ^{18}Mg [25]. This inversion of these orbitals between $N = 8$ and $N = 6$ is well known in the neighboring odd-Z F isotopes [56,67,81–83]. According to the SM calculations, with the proton orbital inversion, the 2_1^+ state in ^{18}Mg mainly arises from the excitation of $\pi 2s_{1/2} \rightarrow \pi 1d_{5/2}$, whereas the 2_1^+ state in ^{20}Mg results from the internal excitation within the $\pi 1d_{5/2}$ orbital. Meanwhile, the neutron configurations in the 2_1^+ states of ^{20}Mg and ^{18}Mg are almost unchanged compared to their ground states. Thus, the relatively higher 2_1^+ excitation energy in ^{18}Mg relative to ^{20}Mg can be ascribed to different excitation characters of the valence protons.

In summary, the invariant-mass reconstructions of ^{20}Mg and ^{19}Mg have been performed and four and five resonant states are identified in these nuclei, respectively. The R_{42} ratio of 2.10(1) in ^{20}Mg reveals a sphere or weakly deformed shape, which excludes the possibility of deformation-driven weakening of the $N = 8$ shell closure. Systematics of $E^*(2_1^+)$ and R_{42} along isotopic and isotonic chains in comparison with the SM calculations using the YSOX interaction suggest the persistence of the $N = 8$ shell around the proton drip-line. The energy difference between the $1/2_1^-$ and $1/2_1^+$ states in ^{19}Mg is compared with its isotones and manifests the magnitude of the $N = 8$ shell. Due to the inversion of $\pi 2s_{1/2}$ and $\pi 1d_{5/2}$ orbitals in the Mg isotopes near the proton drip-line, the higher excitation energy of the 2_1^+ state in ^{18}Mg than this state in ^{20}Mg can be ascribed to their different excitation characters.

We acknowledge Prof. D. Y. Pang for the calculations of reaction cross sections. This work was supported by the National Key R&D Program of China under Grants No. 2022YFA1602302 and No. 2018YFA0404403; the National Natural Science Foundation of China under Grants No. 12035001, No. U2167201, and No. 11975282; the Guangdong Major Project of Basic and Applied Basic Research under Grant No. 2021B0301030006; the U.S. Department of Energy, Office of Science, Office of Nuclear Physics, under Grant No. DE-FG02-87ER-40316; the U.S. National Science Foundation under Grant No. PHY-2209145, and the State Key Laboratory of Nuclear Physics and Technology, Peking University, under Grant No. NPT2020KFY13.

[1] M. G. Mayer, On closed shells in nuclei. II, Phys. Rev. **75**, 1969 (1949).
[2] O. Haxel, J. H. D. Jensen, and H. E. Suess, On the "Magic Numbers" in nuclear structure, Phys. Rev. **75**, 1766 (1949).
[3] C. Détraz, D. Guillemaud, G. Huber, R. Klapisch, M. Langevin, F. Naulin, C. Thibault, L. C. Carraz, and F. Touchard, Beta decay of $^{27-32}$Na and their descendants, Phys. Rev. C **19**, 164 (1979).
[4] E. K. Warburton, J. A. Becker, and B. A. Brown, Mass systematics for $A = 29 - 44$ nuclei: The deformed $A \sim 32$ region, Phys. Rev. C **41**, 1147 (1990).
[5] A. Navin, D. W. Anthony, T. Aumann, T. Baumann, D. Bazin, Y. Blumenfeld, B. A. Brown, T. Glasmacher, P. G. Hansen, R. W. Ibbotson *et al.*, Direct evidence for the breakdown of the $N = 8$ shell closure in ^{12}Be, Phys. Rev. Lett. **85**, 266 (2000).
[6] H. Iwasaki, T. Motobayashi, H. Akiyoshi, Y. Ando, N. Fukuda, H. Fujiwara, Z. Fülöp, K. Hahn, Y. Higurashi, M. Hirai *et al.*, Low-lying intruder 1^- state in ^{12}Be and the melting of the $N = 8$ shell closure, Phys. Lett. B **491**, 8 (2000).
[7] S. D. Pain, W. N. Catford, N. A. Orr, J. C. Angélique, N. I. Ashwood, V. Bouchat, N. M. Clarke, N. Curtis, M. Freer, B. R. Fulton *et al.*, Structure of ^{12}Be: Intruder d-wave strength at $N = 8$, Phys. Rev. Lett. **96**, 032502 (2006).
[8] L. Gaudefroy, O. Sorlin, D. Beaumel, Y. Blumenfeld, Z. Dombrádi, S. Fortier, S. Franchoo, M. Gélin, J. Gibelin, S. Grévy *et al.*, Reduction of the spin-orbit splittings at the $N = 28$ shell closure, Phys. Rev. Lett. **97**, 092501 (2006).
[9] B. Bastin, S. Grévy, D. Sohler, O. Sorlin, Z. Dombrádi, N. L. Achouri, J. C. Angélique, F. Azaiez, D. Baiborodin, R. Borcea *et al.*, Collapse of the $N = 28$ shell closure in ^{42}Si, Phys. Rev. Lett. **99**, 022503 (2007).
[10] H. L. Crawford, P. Fallon, A. O. Macchiavelli, P. Doornenbal, N. Aoi, F. Browne, C. M. Campbell, S. Chen, R. M. Clark, M. L. Cortés *et al.*, First spectroscopy of the near drip-line nucleus ^{40}Mg, Phys. Rev. Lett. **122**, 052501 (2019).
[11] A. Ozawa, T. Kobayashi, T. Suzuki, K. Yoshida, and I. Tanihata, New magic number, $N = 16$, near the neutron drip line, Phys. Rev. Lett. **84**, 5493 (2000).
[12] M. Stanoiu, F. Azaiez, Zs. Dombrádi, O. Sorlin, B. A. Brown, M. Belleguic, D. Sohler, M. G. Saint Laurent, M. J. Lopez-Jimenez, Y. E. Penionzhkevich *et al.*, $N = 14$ and 16 shell

gaps in neutron-rich oxygen isotopes, Phys. Rev. C **69**, 034312 (2004).
[13] D. Cortina-Gil, J. Fernandez-Vazquez, T. Aumann, T. Baumann, J. Benlliure, M. J. G. Borge, L. V. Chulkov, U. Datta Pramanik, C. Forssén, L. M. Fraile *et al.*, Shell structure of the near-dripline nucleus ^{23}O, Phys. Rev. Lett. **93**, 062501 (2004).
[14] A. T. Gallant, J. C. Bale, T. Brunner, U. Chowdhury, S. Ettenauer, A. Lennarz, D. Robertson, V. V. Simon, A. Chaudhuri, J. D. Holt *et al.*, New precision mass measurements of neutron-rich calcium and potassium isotopes and three-nucleon forces, Phys. Rev. Lett. **109**, 032506 (2012).
[15] F. Wienholtz, D. Beck, K. Blaum, C. Borgmann, M. Breitenfeldt, R. B. Cakirli, S. George, F. Herfurth, J. D. Holt, M. Kowalska *et al.*, Masses of exotic calcium isotopes pin down nuclear forces, Nature (London) **498**, 346 (2013).
[16] D. Steppenbeck, S. Takeuchi, N. Aoi, P. Doornenbal, M. Matsushita, H. Wang, H. Baba, N. Fukuda, S. Go, M. Honma *et al.*, Evidence for a new nuclear magic number from the level structure of ^{54}Ca, Nature (London) **502**, 207 (2013).
[17] D. Steppenbeck, S. Takeuchi, N. Aoi, P. Doornenbal, M. Matsushita, H. Wang, Y. Utsuno, H. Baba, S. Go, J. Lee *et al.*, Low-lying structure of ^{50}Ar and the $N = 32$ subshell closure, Phys. Rev. Lett. **114**, 252501 (2015).
[18] M. Rosenbusch, P. Ascher, D. Atanasov, C. Barbieri, D. Beck, K. Blaum, C. Borgmann, M. Breitenfeldt, R. B. Cakirli, A. Cipollone *et al.*, Probing the $N = 32$ shell closure below the magic proton number $Z = 20$: Mass measurements of the exotic isotopes ^{52,53}K, Phys. Rev. Lett. **114**, 202501 (2015).
[19] S. Michimasa, M. Kobayashi, Y. Kiyokawa, S. Ota, D. S. Ahn, H. Baba, G. P. A. Berg, M. Dozono, N. Fukuda, T. Furuno *et al.*, Magic nature of neutrons in ^{54}Ca: First mass measurements of $^{55-57}$Ca, Phys. Rev. Lett. **121**, 022506 (2018).
[20] E. Leistenschneider, M. P. Reiter, S. Ayet San Andrés, B. Kootte, J. D. Holt, P. Navrátil, C. Babcock, C. Barbieri, B. R. Barquest, J. Bergmann *et al.*, Dawning of the $N = 32$ shell closure seen through precision mass measurements of neutron-rich titanium isotopes, Phys. Rev. Lett. **120**, 062503 (2018).
[21] S. Chen, J. Lee, P. Doornenbal, A. Obertelli, C. Barbieri, Y. Chazono, P. Navrátil, K. Ogata, T. Otsuka, F. Raimondi *et al.*, Quasifree neutron knockout from ^{54}Ca corroborates arising $N = 34$ neutron magic number, Phys. Rev. Lett. **123**, 142501 (2019).
[22] H. N. Liu, A. Obertelli, P. Doornenbal, C. A. Bertulani, G. Hagen, J. D. Holt, G. R. Jansen, T. D. Morris, A. Schwenk, R. Stroberg *et al.*, How robust is the $N = 34$ subshell closure? First spectroscopy of ^{52}Ar, Phys. Rev. Lett. **122**, 072502 (2019).
[23] X. Xu, M. Wang, K. Blaum, J. D. Holt, Y. A. Litvinov, A. Schwenk, J. Simonis, S. R. Stroberg, Y. H. Zhang, H. S. Xu *et al.*, Masses of neutron-rich $^{52-54}$Sc and ^{54,56}Ti nuclides: The $N = 32$ subshell closure in scandium, Phys. Rev. C **99**, 064303 (2019).
[24] E. Leistenschneider, E. Dunling, G. Bollen, B. A. Brown, J. Dilling, A. Hamaker, J. D. Holt, A. Jacobs, A. A. Kwiatkowski, T. Miyagi *et al.* (The LEBIT Collaboration and the TITAN Collaboration), Precision mass measurements of neutron-rich scandium isotopes refine the evolution of $N = 32$ and $N = 34$ shell closures, Phys. Rev. Lett. **126**, 042501 (2021).
[25] O. Sorlin and M.-G. Porquet, Nuclear magic numbers: New features far from stability, Prog. Part. Nucl. Phys. **61**, 602 (2008).
[26] T. Otsuka, A. Gade, O. Sorlin, T. Suzuki, and Y. Utsuno, Evolution of shell structure in exotic nuclei, Rev. Mod. Phys. **92**, 015002 (2020).
[27] F. Nowacki, A. Obertelli, and A. Poves, The neutron-rich edge of the nuclear landscape: Experiment and theory, Prog. Part. Nucl. Phys. **120**, 103866 (2021).
[28] D. Suzuki, H. Iwasaki, D. Beaumel, L. Nalpas, E. Pollacco, M. Assié, H. Baba, Y. Blumenfeld, N. De Séréville, A. Drouart *et al.*, Breakdown of the $Z = 8$ shell closure in unbound ^{12}O and its mirror symmetry, Phys. Rev. Lett. **103**, 152503 (2009).
[29] T. Otsuka, R. Fujimoto, Y. Utsuno, B. A. Brown, M. Honma, and T. Mizusaki, Magic numbers in exotic nuclei and spin-isospin properties of the *NN* interaction, Phys. Rev. Lett. **87**, 082502 (2001).
[30] J. S. Randhawa, R. Kanungo, M. Holl, J. D. Holt, P. Navrátil, S. R. Stroberg, G. Hagen, G. R. Jansen, M. Alcorta, C. Andreoiu *et al.*, Observation of excited states in ^{20}Mg sheds light on nuclear forces and shell evolution, Phys. Rev. C **99**, 021301(R) (2019).
[31] Y. Jin, C. Y. Niu, K. W. Brown, Z. H. Li, H. Hua, A. K. Anthony, J. Barney, R. J. Charity, J. Crosby, D. Dell'Aquila *et al.*, First observation of the four-proton unbound nucleus ^{18}Mg, Phys. Rev. Lett. **127**, 262502 (2021).
[32] Z. Ren, Z. Zhu, Y. Cai, and G. Xu, Relativistic mean-field study of Mg isotopes, Phys. Lett. B **380**, 241 (1996).
[33] F. Grümmer, B. Chen, Z. Ma, and S. Krewald, Bulk properties of light deformed nuclei derived from a medium-modified meson-exchange interaction, Phys. Lett. B **387**, 673 (1996).
[34] G. Lalazissis, A. Farhan, and M. Sharma, Light nuclei near neutron and proton drip lines in relativistic mean-field theory, Nucl. Phys. A **628**, 221 (1998).
[35] T. Siiskonen, P. O. Lipas, and J. Rikovska, Shell-model and Hartree-Fock calculations for even-mass O, Ne, and Mg nuclei, Phys. Rev. C **60**, 034312 (1999).
[36] M. V. Stoitsov, J. Dobaczewski, P. Ring, and S. Pittel, Quadrupole deformations of neutron-drip-line nuclei studied within the Skyrme Hartree-Fock-Bogoliubov approach, Phys. Rev. C **61**, 034311 (2000).
[37] G. A. Lalazissis, D. Vretenar, and P. Ring, Relativistic Hartree-Bogoliubov description of sizes and shapes of $A = 20$ isobars, Phys. Rev. C **63**, 034305 (2001).
[38] P. Mitra, G. Gangopadhyay, and B. Malakar, Deformation constrained calculation for light nuclei in generalized hybrid derivative coupling model, Phys. Rev. C **65**, 034329 (2002).
[39] M. V. Stoitsov, J. Dobaczewski, W. Nazarewicz, S. Pittel, and D. J. Dean, Systematic study of deformed nuclei at the drip lines and beyond, Phys. Rev. C **68**, 054312 (2003).
[40] L. Li, J. Meng, P. Ring, E.-G. Zhao, and S.-G. Zhou, Deformed relativistic Hartree-Bogoliubov theory in continuum, Phys. Rev. C **85**, 024312 (2012).
[41] M. K. Gaidarov, P. Sarriguren, A. N. Antonov, and E. Moya de Guerra, Ground-state properties and symmetry energy of neutron-rich and neutron-deficient Mg isotopes, Phys. Rev. C **89**, 064301 (2014).
[42] K. Y. Zhang, D. Y. Wang, and S. Q. Zhang, Effects of pairing, continuum, and deformation on particles in the classically forbidden regions for Mg isotopes, Phys. Rev. C **100**, 034312 (2019).
[43] R. Rodríguez-Guzmán, J. Egido, and L. Robledo, Correlations beyond the mean field in magnesium isotopes: angular

momentum projection and configuration mixing, Nucl. Phys. A **709**, 201 (2002).
[44] Q. Zhi and Z. Ren, Systematic calculations on the ground state properties of Mg isotopes by the macroscopic–microscopic model, Phys. Lett. B **638**, 166 (2006).
[45] S. Ebata, T. Nakatsukasa, and T. Inakura, Systematic investigation of low-lying dipole modes using the canonical-basis time-dependent Hartree-Fock-Bogoliubov theory, Phys. Rev. C **90**, 024303 (2014).
[46] J. Görres, M. Wiescher, and F.-K. Thielemann, Bridging the waiting points: The role of two-proton capture reactions in the *rp* process, Phys. Rev. C **51**, 392 (1995).
[47] M. Wiescher, J. Görres, and H. Schatz, Break-out reactions from the CNO cycles, J. Phys. G: Nucl. Part. Phys. **25**, R133 (1999).
[48] A. Stolz, T. Baumann, T. Ginter, D. Morrissey, M. Portillo, B. Sherrill, M. Steiner, and J. Stetson, Production of rare isotope beams with the NSCL fragment separator, Nucl. Instrum. Methods Phys. Res. Sect. B **241**, 858 (2005).
[49] D. Morrissey, B. Sherrill, M. Steiner, A. Stolz, and I. Wiedenhoever, Commissioning the A1900 projectile fragment separator, Nucl. Instrum. Methods Phys. Res. Sect. B **204**, 90 (2003).
[50] S4 Design by Micron Semiconductor Ltd., http://www.micronsemiconductor.co.uk/product/s4/.
[51] D. Bazin, J. Caggiano, B. Sherrill, J. Yurkon, and A. Zeller, The S800 spectrograph, Nucl. Instrum. Methods Phys. Res. Sect. B **204**, 629 (2003).
[52] J. Yurkon, D. Bazin, W. Benenson, D. Morrissey, B. Sherrill, D. Swan, and R. Swanson, Focal plane detector for the S800 high-resolution spectrometer, Nucl. Instrum. Methods Phys. Res. Sect. A **422**, 291 (1999).
[53] M. Wang, W. Huang, F. Kondev, G. Audi, and S. Naimi, The AME 2020 atomic mass evaluation (II). Tables, graphs and references, Chin. Phys. C **45**, 030003 (2021).
[54] W. Benenson, A. Guichard, E. Kashy, D. Mueller, H. Nann, and L. Robinson, Mass measurements of ^{19}Na and ^{23}Al using the (^{3}He, ^{8}Li) reaction, Phys. Lett. B **58**, 46 (1975).
[55] C. Angulo, G. Tabacaru, M. Couder, M. Gaelens, P. Leleux, A. Ninane, F. Vanderbist, T. Davinson, P. J. Woods, J. S. Schweitzer *et al.*, Identification of a new low-lying state in the proton drip line nucleus ^{19}Na, Phys. Rev. C **67**, 014308 (2003).
[56] I. Mukha, K. Sümmerer, L. Acosta, M. A. G. Alvarez, E. Casarejos, A. Chatillon, D. Cortina-Gil, I. A. Egorova, J. M. Espino, A. Fomichev *et al.*, Spectroscopy of proton-unbound nuclei by tracking their decay products in-flight: One- and two-proton decays of ^{15}F, ^{16}Ne, and ^{19}Na, Phys. Rev. C **82**, 054315 (2010).
[57] S. LaFrance, H. T. Fortune, S. Mordechai, M. E. Cobern, G. E. Moore, R. Middleton, W. Chung, and B. H. Wildenthal, ^{20}O from ^{18}O(t, p), Phys. Rev. C **20**, 1673 (1979).
[58] I. Mukha, L. Grigorenko, L. Acosta, M. A. G. Alvarez, E. Casarejos, A. Chatillon, D. Cortina-Gil, J. M. Espino, A. Fomichev, J. E. García-Ramos *et al.*, New states in ^{18}Na and ^{19}Mg observed in the two-proton decay of ^{19}Mg, Phys. Rev. C **85**, 044325 (2012).
[59] I. Mukha, K. Sümmerer, L. Acosta, M. A. G. Alvarez, E. Casarejos, A. Chatillon, D. Cortina-Gil, J. Espino, A. Fomichev, J. E. García-Ramos *et al.*, Observation of two-proton radioactivity of ^{19}Mg by tracking the decay products, Phys. Rev. Lett. **99**, 182501 (2007).
[60] I. Mukha, L. V. Grigorenko, X. Xu, L. Acosta, E. Casarejos, A. A. Ciemny, W. Dominik, J. Duénas-Díaz, V. Dunin, J. M. Espino *et al.*, Observation and spectroscopy of new proton-unbound isotopes ^{30}Ar and ^{29}Cl: An interplay of prompt two-proton and sequential decay, Phys. Rev. Lett. **115**, 202501 (2015).
[61] X.-D. Xu, I. Mukha, L. V. Grigorenko, C. Scheidenberger, L. Acosta, E. Casarejos, V. Chudoba, A. A. Ciemny, W. Dominik, J. Duénas-Díaz *et al.*, Spectroscopy of excited states of unbound nuclei ^{30}Ar and ^{29}Cl, Phys. Rev. C **97**, 034305 (2018).
[62] I. Mukha, L. Grigorenko, K. Sümmerer, L. Acosta, M. A. G. Alvarez, E. Casarejos, A. Chatillon, D. Cortina-Gil, J. M. Espino, A. Fomichev *et al.*, Proton-proton correlations observed in two-proton decay of ^{19}Mg and ^{16}Ne, Phys. Rev. C **77**, 061303(R) (2008).
[63] L. Ni *et al.*, Decay paths of resonant states in ^{19}Mg (unpublished).
[64] C. Yuan, T. Suzuki, T. Otsuka, F. Xu, and N. Tsunoda, Shell-model study of boron, carbon, nitrogen, and oxygen isotopes with a monopole-based universal interaction, Phys. Rev. C **85**, 064324 (2012).
[65] C. Yuan, C. Qi, F. Xu, T. Suzuki, and T. Otsuka, Mirror energy difference and the structure of loosely bound proton-rich nuclei around $A = 20$, Phys. Rev. C **89**, 044327 (2014).
[66] C. Bertulani and A. Gade, MOMDIS: A Glauber model computer code for knockout reactions, Comput. Phys. Commun. **175**, 372 (2006).
[67] Evaluated Nuclear Structure Data File (ENSDF), http://www.nndc.bnl.gov/ensdf.
[68] K. Marinova, W. Geithner, M. Kowalska, K. Blaum, S. Kappertz, M. Keim, S. Kloos, G. Kotrotsios, P. Lievens, R. Neugart *et al.*, Charge radii of neon isotopes across the *sd* neutron shell, Phys. Rev. C **84**, 034313 (2011).
[69] T. Al Kalanee, J. Gibelin, P. Roussel-Chomaz, N. Keeley, D. Beaumel, Y. Blumenfeld, B. Fernández-Domínguez, C. Force, L. Gaudefroy, A. Gillibert *et al.*, Structure of unbound neutron-rich ^{9}He studied using single-neutron transfer, Phys. Rev. C **88**, 034301 (2013).
[70] G.-B. Liu and H. T. Fortune, ^{9}Be(t, p)^{11} Be and the structure of ^{11}Be, Phys. Rev. C **42**, 167 (1990).
[71] F. Ajzenberg-Selove, Energy levels of light nuclei $A = 13$–15, Nucl. Phys. A **523**, 1 (1991).
[72] P. G. Sharov, A. S. Fomichev, A. A. Bezbakh, V. Chudoba, I. A. Egorova, M. S. Golovkov, T. A. Golubkova, A. V. Gorshkov, L. V. Grigorenko, G. Kaminski *et al.*, Search for 2*p* decay of the first excited state of ^{17}Ne, Phys. Rev. C **96**, 025807 (2017).
[73] K. K. Seth, M. Artuso, D. Barlow, S. Iversen, M. Kaletka, H. Nann, B. Parker, and R. Soundranayagam, Exotic nucleus helium-9 and its excited states, Phys. Rev. Lett. **58**, 1930 (1987).
[74] R. Kanungo, A. Andreyev, L. Buchmann, B. Davids, G. Hackman, D. Howell, P. Khalili, B. Mills, E. P. Rodal, S. C. Pieper *et al.*, Spectroscopic factors for the ^{9}Li ground state and $N = 6$ shell closure, Phys. Lett. B **660**, 26 (2008).
[75] T. Moriguchi, A. Ozawa, S. Ishimoto, Y. Abe, M. Fukuda, I. Hachiuma, Y. Ishibashi, Y. Ito, T. Kuboki, M. Lantz *et al.*, Density distributions of ^{11}Li deduced from reaction cross-section measurements, Phys. Rev. C **88**, 024610 (2013).
[76] H. Iwasaki, T. Motobayashi, H. Akiyoshi, Y. Ando, N. Fukuda, H. Fujiwara, Z. Fülöp, K. Hahn, Y. Higurashi, M. Hirai *et al.*, Quadrupole deformation of ^{12}Be studied by proton inelastic scattering, Phys. Lett. B **481**, 7 (2000).

[77] J. Chen, J. Lou, Y. Ye, Z. Li, D. Pang, C. Yuan, Y. Ge, Q. Li, H. Hua, D. Jiang *et al.*, A new measurement of the intruder configuration in ^{12}Be, Phys. Lett. B **781**, 412 (2018).

[78] C. Morse, E. McCutchan, H. Iwasaki, C. Lister, V. Bader, D. Bazin, S. Beceiro Novo, P. Chowdhury, A. Gade, T. Johnson *et al.*, Enhanced collectivity in ^{12}Be, Phys. Lett. B **780**, 227 (2018).

[79] Y. Kanada-En'yo, Breaking of $N = 8$ magicity in ^{13}Be, Phys. Rev. C **85**, 044320 (2012).

[80] H. Iwasaki, A. Dewald, C. Fransen, A. Gelberg, M. Hackstein, J. Jolie, P. Petkov, T. Pissulla, W. Rother, and K. O. Zell, Low-lying neutron intruder state in ^{13}B and the fading of the $N = 8$ shell closure, Phys. Rev. Lett. **102**, 202502 (2009).

[81] H. T. Fortune, Constraints on energies of ^{15}F(g.s.), ^{15}O($\frac{1}{2}^+, t = \frac{3}{2}$), and ^{16}F($0^+, t = 2$), Phys. Rev. C **74**, 054310 (2006).

[82] F. de Grancey, A. Mercenne, F. de Oliveira Santos, T. Davinson, O. Sorlin, J. Angélique, M. Assié, E. Berthoumieux, R. Borcea, A. Buta *et al.*, An above-barrier narrow resonance in ^{15}F, Phys. Lett. B **758**, 26 (2016).

[83] A. Morton, J. Chow, J. King, R. Boyd, N. Bateman, L. Buchmann, J. D'Auria, T. Davinson, M. Dombsky, W. Galster *et al.*, Beta-delayed particle decay of ^{17}Ne, Nucl. Phys. A **706**, 15 (2002).